Bioorganic & Medicinal Chemistry 18 (2010) 6805–6812

Contents lists available at ScienceDirect

Bioorganic & Medicinal Chemistry

journal homepage: www.elsevier.com/locate/bmc

Insights into MAPK p38α DFG flip mechanism by accelerated molecular dynamics

Federico Filomia [a], Francesca De Rienzo [a,b], M. Cristina Menziani [a,*]

[a] Department of Chemistry, University of Modena & Reggio Emilia, Italy—Via Giuseppe Campi 183, 41100 Modena, Italy
[b] INFM-CNR National Center on nanoStructures and bioSystems at Surfaces (S3)—Via Campi 213/A, 41100 Modena, Italy

ARTICLE INFO

Article history:
Received 2 April 2010
Revised 16 July 2010
Accepted 20 July 2010
Available online 29 July 2010

Keywords:
p38 MAPKinase
DFG-loop
Allosteric inhibitors
Molecular dynamics simulation
Conformational change
Mechanism

ABSTRACT

The DFG motif at the beginning of the activation loop of the MAPK p38α undergoes a local structural reorganization upon binding of allosteric type-II and type-III inhibitors, which causes the residue F^{169} to move from a buried conformation (defined as DFG-in) to a solvent exposed conformation (defined as DFG-out). Although both experimental and computer simulation studies had been performed with the aim of unveiling the details of the DFG-in to DFG-out transition, the molecular mechanism is still far from being unequivocally depicted.

Here, the accelerated molecular dynamics (AMD) technique has been applied to model the active loop flexibility of p38α and sample special protein conformations which can be accessible only in some conditions or time periods. Starting from the assumption of an experimentally known initial and final state of the protein, the study allowed the description of the interaction network and the structural intermediates which lead the protein to change its loop conformation and active site accessibility. Besides a few important hydrogen bond interactions, a primary role seems to be played by cation–π interactions, involving the DFG-loop residue F^{169}, which participate in the stabilization of an intermediate conformation and in its consequent transition to the DFG-out conformation. From this study, insights which may prove useful for inhibitor design and/or site directed mutagenesis studies are derived.

1. Introduction

The p38α proteins belong to the mitogen-activated protein kinases (MAPKs), a super-family of enzymes that is involved in many critical cellular processes such as proliferation, apoptosis and differentiation.[1] Their activation mechanism is based on a dual phosphorylation reaction taking place on specific threonine and tyrosine residues belonging to the flexible activation loop responsible for the opening and the closing of the binding cavity,[2,3] where one ATP molecule binds during the activation process (see Fig. 1a).

The activation loop carries a DFG (Asp-Phe-Gly) motif, largely conserved among most of the proteins belonging to the kinase protein super-family.[4] The conformations assumed by this flexible loop (or DFG-loop) are mainly characterized by the shift of the F side-chain (F^{169} in the p38α protein) from its usual buried conformation (DFG-in) (see Fig. 1b) to a conformation that sterically interferes with ATP binding (DFG-out) (see Fig. 1c and d).

To date, a large number of completely resolved DFG-in three-dimensional structures, both in their apo and ligand-complexed forms, are collected in the RSCB Protein Data Bank,[5] thus simplifying the development of new drugs designed to compete with ATP binding (type-I inhibitors[6–8]) (Fig. 1b). On the contrary, the number of published DFG-out three-dimensional structures with the activation loop completely resolved is not as significant. Moreover, until now, this latter conformation of the loop has been experimentally observed only in the presence of particular inhibitors based on a modified urea or amide scaffold capable to bind meanwhile to the ATP site and to a nearby allosteric hydrophobic pocket which becomes accessible by the flip of the DFG-loop (type-II inhibitors[9]) or exclusively within the allosteric pocket (type-III inhibitors[10]) (Fig. 1c and d). The urea/amide moiety of the allosteric inhibitors is considered to be fundamental for the DFG flip[11] triggered by the establishment of two specific H-bonds with residues D^{168} (belonging to the activation loop) and residue E^{71} (belonging to Helix-C).[12,13]

Whereas the hypothesis of a DFG-out conformation induced by allosteric inhibitors is generally supported by the results of X-ray experiments and by their slow binding kinetics experimentally observed,[14,12] the existence of a dynamic equilibrium between the DFG-in and DFG-out conformations of p38α in its apo and complexed form has been first advanced on the basis of the results of NMR studies.[15] The authors hypothesize that the DFG-out state is sampled less frequently than the DFG-in conformation; type-II inhibitors bind to the DFG-out form, freezing the protein in this conformation and suppressing the conformational exchange, while

* Corresponding author. Tel.: +39 059 2055091; fax: +39 059 373543.
E-mail address: menziani@unimore.it (M.C. Menziani).

0968-0896/$ - see front matter © 2010 Elsevier Ltd. All rights reserved.
doi:10.1016/j.bmc.2010.07.047

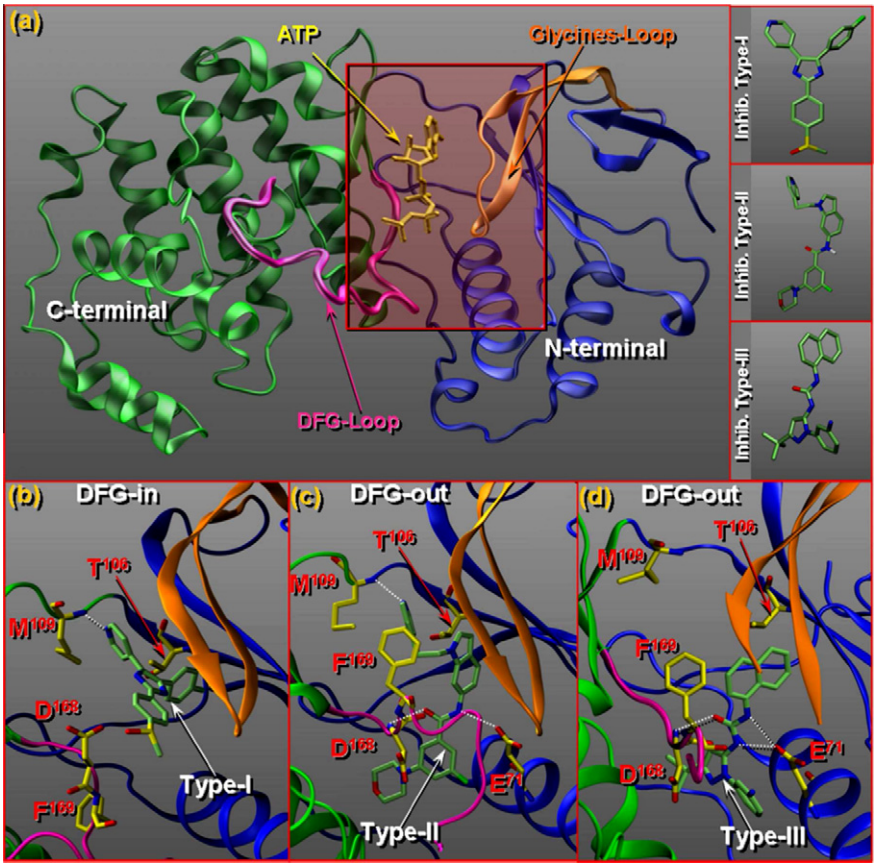

Figure 1. Cartoon representation of the DFG-in p38α structure (PDB ID: 1P38) (a). The important features of the enzyme and the binding site are highlighted. Focus on the binding site of (b) DFG-in p38α structure in complex with type-I inhibitor (PDB ID: 1A9U), (c) DFG-out p38α structure in complex with type-II inhibitor (PDB ID: 1WBT), (d) DFG-out p38α structure in complex with type-III inhibitor (PDB ID: 3HV7). All figures were prepared with VMD software.[32]

the binding of traditional inhibitors (ATP-site binders) affects the DFG equilibrium to a lesser extent. Besides NMR, Molecular Dynamics (MD) simulations are also being used extensively to sample the accessible protein conformations and build adequate pharmacophoric models. In particular, the dynamic behaviour of the DFG-loop was taken into account in a recent paper by Fremberg-Kesner and Elcock,[16] who applied a high temperature (HT) molecular dynamics simulation to fasten the DFG-in to DFG-out transition and back, combined with a docking protocol to analyze the ligand binding properties of the different conformations. They described the presence of two transitional conformations defined as pseudo-DFG-in and pseudo-DFG-out, due to their respective similarity to the DFG-in and DFG-out states, and demonstrated that type-II inhibitors are able to bind not only to the p38α DFG-out state but also to its DFG-in state. Thus, this observation supports the hypothesis that the pre-existence of the DFG-out conformation is not a prerequisite for inhibitor binding to p38α, rather the DFG-out conformation might be triggered by the initial binding of type-II-inhibitor into the DFG-in conformation.

Recently, a detailed interpretation of the DFG flip in the Abl kinase has been given in the paper by Shana et al.[17] Here, a combined experimental and theoretical approach, was applied to demonstrate that the DFG flip is regulated by the protonation of the DFG-loop aspartate residue; this allows the formation of a H-bond between the aspartate side-chain and the backbone carbonyl of a nearby valine, which promotes the DFG-loop conformational switch. Also in this work, evidence is provided for the existence of a stable intermediate conformation, which allows binding of a specific DFG-out binder inhibitor.

This thesis finds support in other computational and experimental studies recently performed. In particular, Kufareva and Abagyan,[9] by applying a structure-based approach to design and evaluate type-II kinase inhibitors, demonstrated that the determinants for allosteric binding are preserved in most DFG-in structures. In 2007, an experimental analysis of the DFG conformational transition in p38α has been attempted by Bukhtiyarova et al.[18] They classified five p38α DFG-motif mutants (F169G, F169R, F169Y, F169A and D166G) according to their local DFG conformation and, beside pointing out the determinant role played by residue F^{169} in the structural dynamics of the activation loop, they suggested the existence in the free protein of a peculiar spatial organization, called α-DFG-out, which could be intended as an intermediate between the DFG-in and the DFG-out conformations and which could provide a transient root of entry for type-II inhibitors. Similar intermediate conformations, also named DFG-'in between', were found depending on the structure of the ligands co-crystallized with the p38α proteins manipulated in positions different from the DFG-motive and under different crystallization conditions.[19–21,10] In summary, two mechanisms have been up to now envisaged in the literature for allosteric inhibitors: (1) exclusively binding to proteins in the DFG-out conformation, which, although sampled less frequently, exists in equilibrium with the DFG-in conformation; (2) initial binding to proteins in the DFG-in conformation with subsequent promotion of the DFG-in to -out transition. Besides the recent evidences brought to support this second thesis, no description of the mechanism at the atomic level has yet produced.

In this work, a computational procedure, based on an Accelerated Molecular Dynamics (AMD) technique, will be applied to the human p38α protein, in order to highlight the main interactions which take part in the DFG-in to DFG-out conformational change triggered by the binding of allosteric inhibitors. A viable transition

mechanism will be proposed and implications to drug design will be discussed.

2. Materials and methods

The accelerated molecular dynamics technique, as implemented in GROMACS 3.3.3,[22–24] has been applied to neglect non-energetically convenient pathways by driving the system to a pre-defined direction.

The X-ray structure of p38α from mouse (PDB ID: 1P38) was chosen as the starting conformation since the whole structure is resolved. First, this structure was changed to the human sequence by computationally mutating H^{48} and A^{263} into L^{48} and T^{263}, respectively, with the software QUANTA (Accelrys[25]). The protein was subsequently solvated by 26188 water molecules (SPCE model) to reach an overall system density of 1 gr/l, using the Gromacs software. The solvation box was built using a water buffer which extends 15 Å along each cartesian coordinate starting from the farest atom from the protein centre of mass. Periodic boundary conditions were implemented: a NPT ensemble was simulated and constant temperature (300 K) and pressure (1 atm) were controlled by the Berendsen algorithm.

All calculations were carried out using the Gromacs 3.3.3 suite and the GROMOS'96 force field on a Dual-Core AMD Opteron 64 bit cluster. Short range interactions were treated with the Lennard-Jones potential using a cut-off of 10 Å, while long range interactions were calculated using the PME algorithm within a radius of 10 Å and an interpolation order of 4. In general, ionizable residues were assigned standard protonation states corresponding to pH 7; the solvent-exposed histidines (resid: 64, 77, 80, 107, 142, 174, 228, 305) were protonated and one Na^+ ion was added to the solvent for the system neutrality. All covalent distances were restrained with the LINCS algorithm.[26] The calculation procedure consisted of three main steps: (i) initial minimization (Steepest Descent followed Conjugated Gradient) to reduce the close contacts among water molecules, with all atoms of both protein and inhibitor restrained, using a force constant of 1000 kJ mol^{-1} $Å^{-1}$; (ii) smooth dynamics with all atoms of protein and inhibitor restrained, with a force constant of 1000 kJ mol^{-1} $Å^{-1}$, to remove close contacts between protein and inhibitor atoms and water molecules; (iii) accelerated dynamics with no restraints, run for a total of 6878 ps (with a 0.002 ps time step) made of four sequential full dynamics steps, during which different acceleration vectors were applied. Interaction energies were computed with the CHARMM software,[27] between all residue pairs belonging to the activation loop in proximity of the DFG motif (residues 166–174) and to the nearest binding site residues, to highlight the most relevant interactions involved in and/or promoting the DFG conformational transition.

The ϕ and ψ angle values of D^{168} were computed with the software Discovery Studio 2.5 (Accelrys[28]) from the available crystallographic structures and for a few structures obtained from the simulation.

Two inhibitors solved crystallographically in complex with the p38α enzyme were selected as representative of type-II (PDB ID: 1WBT) and type-III (PDB ID: 3HV7) allosteric binders in order to test the suitability of the mechanism proposed for DFG flip with their binding modalities.

2.1. The accelerated molecular dynamics protocol

The approach exploited here assumes that the conformational change DFG-in/out is induced by the allosteric inhibitors. In this framework, to study the DFG-in/out conformational change with the AMD technique, it is assumed that: (i) in the starting conformation (the DFG-in), F^{169} is buried in its hydrophobic pocket, placed in proximity of the ATP binding site (Fig. 1b), as determined by X-ray structures (PDB ID: 1P38, apo structure); (ii) in the final conformation (the DFG-out), F^{169} is exposed to the solvent and competes with ATP for the binding site, as shown by the corresponding X-ray structures (PDB ID: 1WBT, protein-type-II inhibitor complex) (Fig. 1c); (iii) during the DFG-in to DFG-out transition, F^{169} has a fan-out shaped motion as described in the paper by Frembgen-Kesner and Elcock.[16]

Thus, in the AMD simulations, the forces to be applied to simulate the DFG-in/out conformational transition induced by allosteric inhibitors, were guessed on the basis of the known initial conformation (DFG-in) of the unbound protein, and of the final conformation assumed by the protein when allosteric inhibitors are bound into the active site (DFG-out). For this reason, and because of the non linear displacement that the protein side-chains undergo during the conformational change, the direction of the steering vectors needed to be re-modulated at each AMD step. The Gromacs software allowed the use of several acceleration vectors during each calculation, but their versus and modules needed to be fixed at the beginning and cannot be changed, therefore to simulate a non-linear displacement, several subsequent AMD simulations were carried out. Within each accelerated run, two pulling vectors were applied at the same time to the systems. Vector modules and directions were further accepted or rejected based on: magnitude of the force applied and structural factors, such as conservation of secondary structure of the protein, deformation of the protein. Thus, for each production run, different vectors were tried and rejected until the required final conformation was achieved by a fan-shaped movement of F^{169}. The effective acceleration vectors finally used to control the DFG motif movements during the whole simulation are reported in Table 1. Vectors were applied to all side-chain atoms belonging to F^{169} and D^{168} residues.

3. Results and discussion

The results of the AMD simulations performed in this work are analyzed to obtain a picture of the interaction network and the structural intermediates which lead the protein to change its active site conformation. The study is based on the assumption of fan-shaped motion of F^{169} during the DFG transition between the initial DFG-in and final DFG-out states determined by X-ray crystallography.

3.1. Structural analysis: the pseudo-DFG-out conformation

Analysis of the AMD simulations allowed the description of the dynamic behaviour of the protein MAPK p38α. Fig. 2 shows the root mean square displacement (RMSD) of the protein atoms belonging to the DFG motif, calculated with respect to the corresponding atoms of the initial DFG-in conformation for each MD simulation snapshot. RMSD was calculated by taking into account all the atoms belonging to the DFG motif (red curve) or only the atoms of the DFG backbone (blue curve).

Table 1
Sequence of the acceleration vectors (components, module) applied during the MD simulation.

Step	(x,y,z), Module (nm/ps^2)	
	D^{168}	F^{169}
I	(1.0, 0.0, 1.0), 1.41	(−0.3, 3.0, −0.3), 3.03
II	(0.0, 1.2, 8.0), 8.09	(0.0, 1.2, −8.0), 8.09
III	(0.0, 1.2, 5.0), 5.14	(−5.5, −7.0, −3.5), 9.57
IV	(6.0 0.0 −2.0), 6.32	(−7.5 −12.0 −7.5), 16.02

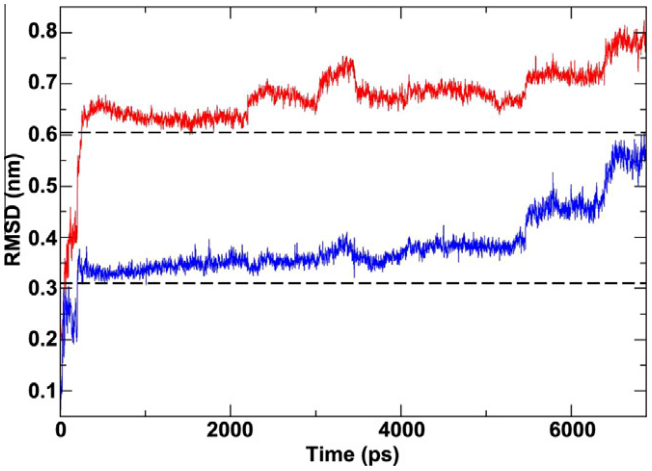

Figure 2. RMSD value evolution: RMSD value of all the DFG motif atoms (red curve, RMSD-in) and backbone DFG motif atoms (blue curve) calculated with respect to the corresponding atoms in the initial DFG-in conformation (PDB ID: 1P38), during the AMD simulation.

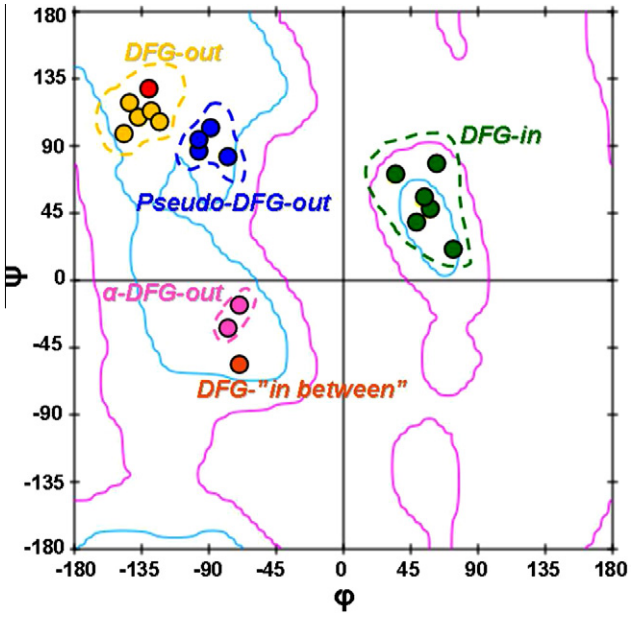

Figure 3. Ramachandran plot for the ϕ and ψ angles of D^{168} in the experimental (yellow; PDB ID: 1WBT, 1WBN, 1W82, 1W83, 1WBS and computed (red) p38α DFG-out conformation; in the experimental p38α DFG-in conformation (green; PDB ID: 1P38, 3D7Z, 3DS6, 2ZAZ, 1BMK, 1BL6); in the X-ray structures of a representative crystal complex (orange; PDBID: 3IW6) and in the DFG mutants F169G and F169R (pink; PDBID: 2PV8 and 2PTJ), which present DFG intermediate conformations, named DFG-'in between' and α-DFG-out, respectively; and in the computed pseudo-DFG-out conformation (blue). The inner contours (cyan) enclose preferred conformational regions, and the outer contours (pink) enclose allowed regions for all amino acids but prolines and glycines.

The red curve, hereafter referred to as RMSD-in, shows that the RMSD moves from about 0.2 nm (initial DFG-in state) to about 0.8 nm (final DFG-out state).

By analysis of the trend of the RMSD-in plot, a plateau can be observed between 500 and 2200 ps: this can be ascribed to the presence of a particular conformation, intermediate between the DFG-in and the DFG-out conformations, which origins during the conformational transition. From 2200 to 4000 ps, the RMSD assumes higher values oscillating around 0.7 nm: this increment is due to a small displacement of the DFG motif that nevertheless preserves the intermediate conformation. From 4000 ps till the end of the simulation, the DFG-loop moves to the DFG-out state, through three successive shifts of the DFG-loop toward the solvent. The final DFG-out state is considered to be reached when the RMSD-in ranges around 0.8 nm.

The dihedral angle (ϕ and ψ) values of residue D^{168} can be exploited to classify the allowed conformations of the activation loop.[18] These values have been determined for: (i) the DFG-in crystallographic p38α structures (PDB ID: 1P38, 3D7Z, 3DS6, 2ZAZ, 1BMK,1BL6); (ii) the DFG-out crystallographic structures (PDB ID: 1WBT, 1WBN, 1W82, 1W83, 1WBS); (iii) the X-ray structures of a representative crystal complex (PDBID: 3IW6) and DFG mutants F169G and F169R (PDBID: 2PV8 and 2PTJ), which present DFG intermediate conformations (named DFG-'in between' and α-DFG-out, respectively and (iv) a set of four snapshots representative of the intermediate conformation in the AMD simulation (time range 500–4000 ps).

They are reported in the Ramachandran plot in Fig. 3. Analysis of the Ramachandran plot shows that the local conformational change from the DFG-in to the DFG-out transition is mainly captured by the $D^{168}\phi$ angle, whose variation is in the range 80° to −135°, while the ψ angle ranges between 20° and 135°.

The DFG-in cluster of X-ray determined structures (Fig. 3, green dots) is the cluster with the largest variation of the D^{168} ψ angle, which can be mainly ascribed to different small local distortion of the DFG backbone, as it is shown in Fig. 4a.

The final DFG-out conformation (Fig. 3, red dot) obtained in the range 6500–6878 ps of the AMD trajectory, can be considered to belong to the DFG-out conformation cluster of X-ray determined structures (Fig. 3, yellow dot), thus clearly indicating that the final DFG-out conformation has been indeed reached. For comparison purposes, the superposition of the X-ray and the computed DFG-out structures is reported in Fig. 4c.

The most representative intermediate conformations sampled in time range 500–4000 ps of the AMD trajectory (Fig. 3, blue dots) occupy the same Ramachandran region of the DFG-out cluster forming nonetheless a clearly distinct group. More precisely, the $D^{168}\psi$ angle is very similar to that observed for the protein conformations in the DFG-out cluster, while the ϕ angle is different, underlying that a complete transition from the DFG-in to the DFG-out conformation has not yet been reached. The intermediate conformation, named pseudo-DFG-out, is depicted in Fig. 4b, where the superposition of the four sampled structures is shown. It is worth noting that the orientation of F^{169} in this conformation is approximately perpendicular to that observed in both the DFG-out and the DFG-in conformations.

A detailed comparison with the pseudo-DFG-out previously described by Frembgen-Kesner and Elcock[16] is difficult since neither the three-dimensional structure nor the D^{168} ϕ and ψ angles are available for this protein conformation; apparently residue L^{171} occupies the room vacated by F^{169} in the binding site pocket, which is not the case in the AMD pseudo-DFG-out structure.

Moreover, the Ramachandran plot in Fig. 3 shows that the local conformation of the DFG motif in the AMD computed pseudo-DFG-out conformation is different from the α-DFG-out conformations found in the mutants F169G and F169R described by Bukhtiyarova et al.,[18] and from the DFG-'in between' conformation found in some crystal complexes,[19–21,10] where the ϕ angle is in the range −60° to −70° and the ψ is in the range −25° to −55°. The portion of the DFG loop at the N-terminal side of the DFG motive is not completely resolved in these crystal structures, however, a visual inspection of the resolved chain segments reveals that in all the structures the loop is prone to assume a conformation which is very similar among the crystal structures but very different from the AMD pseudo-DFG-out. Indeed, the spatial position of the F^{169} and D^{169} side-chains seem to suggest that these structures might

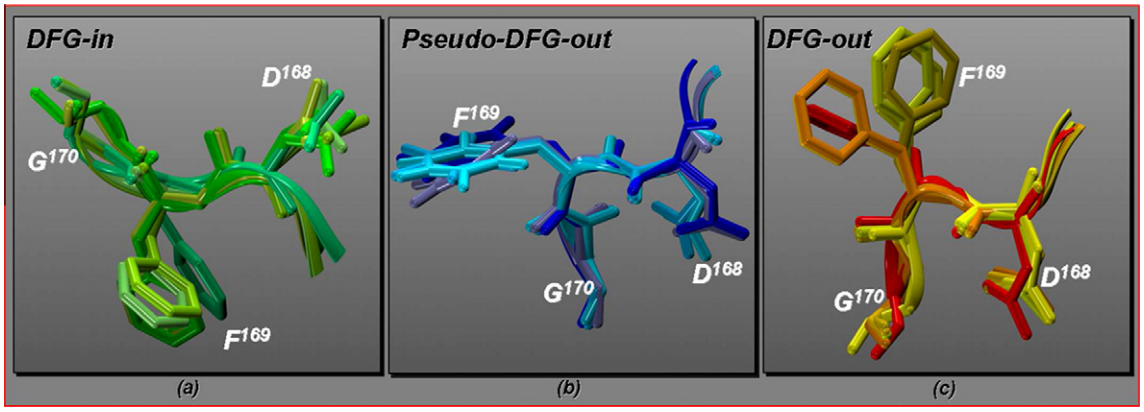

Figure 4. Superimposition of: (a) DFG-in structures PDB ID: 1P38, 3D7Z, 3DS6, 2ZAZ, 1BMK, 1BL6; (b) pseudo-DFG-out structures (snapshots captured in the range 500–4000 ps of the AMD dynamics); (c) DFG-out structures calculated (red), and PDB ID: 1WBT, 1WBN, 1W82, 1W83, 1WBS.

depict an early step of a different pathway in the DFG-in/DFG-out transition determined either by crystallization conditions, protein manipulations or binding of specific ligands. However, the lack of detailed three-dimensional information on the remain of the loop prevent the elaboration of further mechanistic hypothesis.

The DFG loop is also not completely resolved in the crystal structures of the mutants F169G and F169R (PDB ID: 2PV8 and 2PTJ, respectively), however, a visual inspection reveals that the mutated loop is prone to assume a conformation (named α-DGF-out by the Authors) which is very different from the AMD pseudo-DFG-out.

Whether these conformations are commonly accessible by the native protein in its unbound state or only by particular DFG-loop mutants or upon type-II inhibitors binding has not yet been assessed. It is worth stressing, however, that different recent studies agree on the existence of some kind of intermediate stable conformations for the MAPK p38α, which seem to be directly involved in the protein inhibition mechanism: these conformations could constitute the route of entry for allosteric inhibitors and could be therefore exploited for designing new specific inhibitor compounds.

4. The inter-residue interactions involved in the DFG flip

The analysis of the interaction energies (IE) between residues in the binding site region, together with detailed visual inspections of the protein structure conformations along the whole simulations, allow the determination of the main interactions responsible for the DFG-in/out transition.

The initial DFG-in conformation is characterized by the presence of two H-bonds between two residues of the DFG loop (L^{167} and G^{170}) and one residue (H^{145}) belonging to the C-terminal domain. By analyzing the whole trajectory, other five H-bonds (reported in Table 2) can be recognized as important for the studied conformational changes (all the residues involved in these interactions are shown in Fig. 5r/s).

The values of the H-bond distances for HB_1 to HB_5 and their relative H-bond IE were compared with the RMSD-in, calculated with respect to all atoms belonging to the DFG-in motif, in the plots of Fig. 5.

Plot in Fig. 5a highlights that HB_1 length oscillates around 0.25 nm in the range 500–4000 ps, and in the range 0.6–0.8 nm both at the beginning of the simulation (0–500 ps), when the protein is in its DFG-in state and at the in the final part of the simulation (4500–6878 ps), when the protein is in its DFG-out state. Accordingly, fluctuations of the interaction energy (Fig. 5b) between −3 and −4.5 kcal/mol in the time range 500–4000 ps are observed. Therefore, the interaction HB_1 seems to be directly related to the stabilization of the intermediate conformation, existing only during the pseudo-DFG-out conformation life-time. Interestingly, the HB_2 interaction (Fig. 5c) is already present in the DFG-in conformation and it is maintained and optimized in a time range (0–4000 ps) which overlaps the life-time of the pseudo-DFG-out conformation. Its length oscillates, in this interval, from an initial value of 0.3 nm to a value of 0.2 nm with a mean interaction energy value of −4 kcal/mol (Fig. 5d).

Table 2
H-bonding interactions involved in the DFG-loop conformational change and location of the H-bonded pairs in the protein structure and DFG-loop.

ID	Donor acceptor	Location		DFG-loop
		Protein loop	Loop loop	
HB_1	$H_{R173} - O_{R173}$		X	Pseudo
HB_2	$H_{R173} - O_{F169}$		X	In + pseudo
HB_3	$H_{L171} - OD2_{D168}$		X	Pseudo + out
HB_4	$H_{R173} - O_{G170}$		X	In + pseudo
HB_5	$H_{D168} - O_{D150}$	X		Pseudo + out

The analysis of the variation of both the HB_3 length and its IE (see Fig. 5e/f) reveals that this H-bond, not present in the DFG-in conformation, is established in the early stages of the conformational evolution and it is potentially persistent during the whole simulation. In the range 500–2100 ps, the HB_3 length oscillates between 0.2 and 0.3 nm, with an IE ranging between 0 and −6 kcal/mol; afterwards, in the range 2100–4500 ps, HB_3 assumes a length mean value of 0.2 nm, with the IE remaining almost constant at −4 kcal/mol. Then the interaction assumes the same behaviour of the first interval oscillating into the range of 0.2–0.3 nm and the energy decreases until the DFG-out state is reached.

A large variation (0.2–0.4 nm) is observed for HB_4 distance at the beginning of the simulation (Fig. 5g); however, at around 4000 ps, the distance between the hydrogen bonded atoms reaches the value of 0.2 nm which persists until the DFG-loop moves to its final DFG-out conformation. This trend is confirmed by the variation of the IE plot in Fig. 5h: here, the H-bond strength has a negative mean value of about −2 kcal/mol at the beginning of the simulation (0–1700 ps), it decreases in the range 1700–4000 ps and again moves to a lower value of about −4 kcal/mol during the final part of the DFG-in/out transition simulation.

The two hydrogen bonded atoms involved in HB_5 formation (Fig. 5i) belong to the DFG-loop and to the C-terminal domain. The bond length becomes significant for the interaction after 200 ps, remaining constant at around 0.2–0.3 nm along the whole

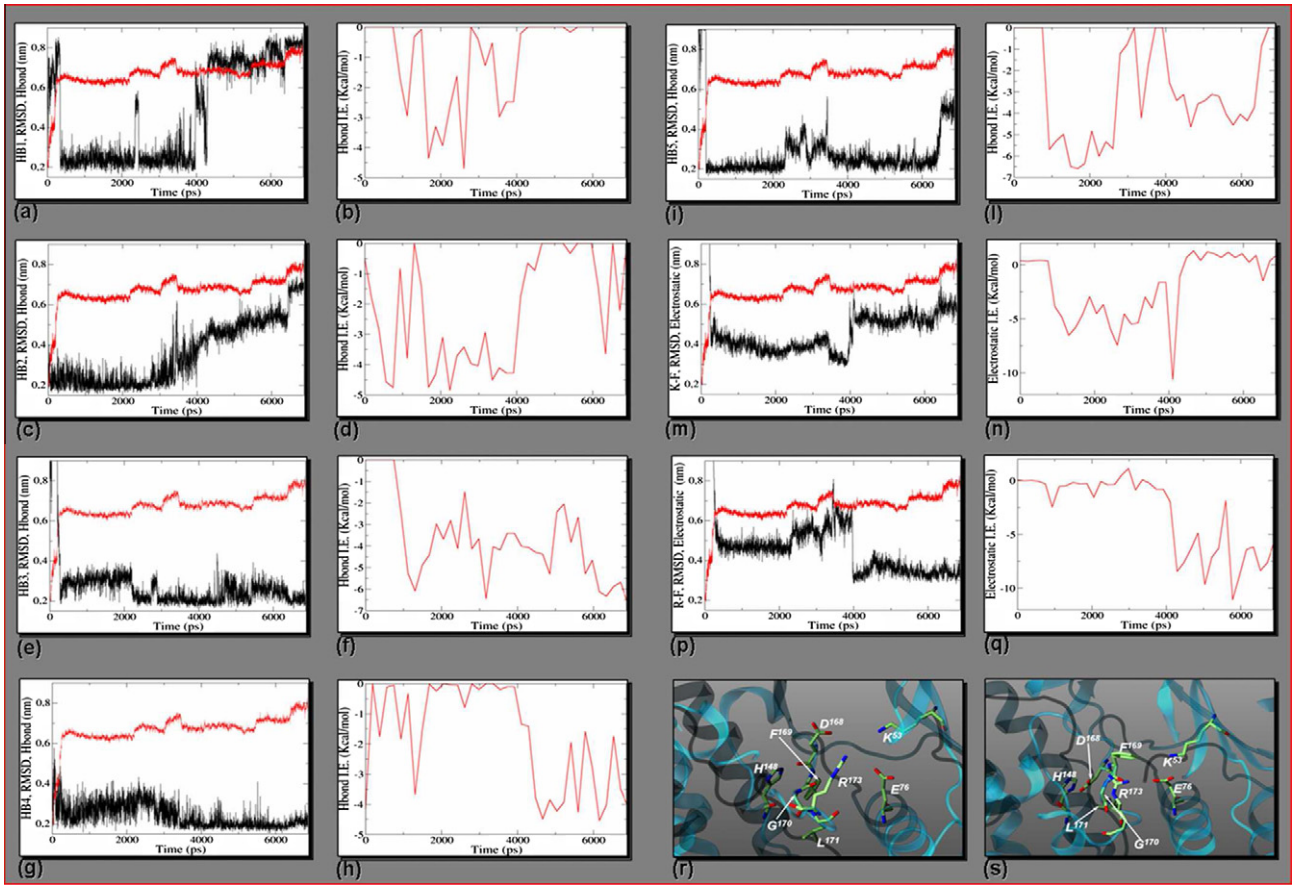

Figure 5. Double line plots—comparison between the RMSD-in (red line) and the H-bond length variation (black line) of HB_1 (a), HB_2 (c), HB_3 (e), HB_4 (g), HB_5 (i), $K^{53} - F^{169}$ cation–π (m) and $R^{173} - F^{169}$ cation–π (p) during the simulation. Single red line plots—interaction energy (IE) plots of interactions HB_1 (b), HB_2 (d), HB_3 (f), HB_4 (h), HB_5 (i), $K^{53} - F^{169}$ cation–π (m) and $R^{173} - F^{169}$ cation–π (p) during the simulation. Residues involved in the H-bond and in the cation–π interactions in the DFG-in (r) and DFG-out (s) conformations (colour code: C atoms: green; N atoms: blue; O atoms: red; H atoms white; cartoon representation of the protein secondary structure: cyan).

simulation, with the exception of the 2500–3500 ps range, where the loop starts to move up toward the entrance of the binding cavity. Also in this case, the behaviour is confirmed by the trend of the energy plot in Fig. 5l: IE assumes very negative values (mean value −6.0 kcal/mol) from 1500 to 2500 ps, it drops to 0 kcal/mol in the time interval between 2500 and 3500 ps, and then the value increases until it reaches the mean value of about −4 kcal/mol in the last part of the simulation.

Besides H-bonds, other interactions seems to be involved in the conformational change. Among the most interesting ones, two cation–π interactions between F^{169} and K^{53} and F^{169} and R^{173} are observed.

The variation of distance between the centre of mass of F^{169} side-chain and the NH_3^+ nitrogen of K^{53} is compared to the RMSD-in plot in Fig. 5m and its electrostatic energy variation is reported in Fig. 5n. These plots show that the interaction is maximized at about 4000 ps, where the distance is about 0.35 nm and the IE is −10 kcal/mol (with a mean value of −5 kcal/mol in the range 500–4000 ps). After that, the interaction becomes much weaker, until the residues involved reach a distance value of about 0.6 nm and the interaction becomes almost repulsive. At this point a new interaction between F^{169} and R^{173} (Fig. 5p/q) is established. Its mean length is about 0.35 nm, and its electrostatic IE mean value can be quantified about −7.5 kcal/mol: in this second part of the simulation, this interaction is more persistent than the previous one.

4.1. The transition mechanism

From the detailed analysis of the main local conformations assumed by the DFG-loop during the AMD study, it is possible to infer the conformational mechanism described in the following.

In the DFG-in state the F^{169} is buried in a hydrophobic pocket placed in proximity of the ATP binding region (Fig. 1b). In this conformation, the activation loop is hydrogen bonded to the C-terminal domain through the interactions established among residue H^{145} (C-terminal region) and residues L^{167} and G^{170} (DFG-loop) (Fig. 6a), and the active site is easily accessible by one molecule of ATP (or one inhibitor molecule). The two hydrogen bond interactions force the loop to assume a particular three-turn fold, which seems to be relevant for all kinase proteins.[4] According to the assumption made in this work, allosteric inhibitor binding causes the exit of F^{169} from its pocket toward the solvent (Fig. 6a and b). The movement of the F^{169} side-chain triggers an overall rearrangement of the DFG-loop which results in the rotation of the D^{168} towards the binding site.

The new orientation of D^{168} allows new H-bonds to be established in substitution of the H-bonding interactions present in the DFG-in conformation, so that the local three-turn conformation of the loop is now kept by two new H-bonds: HB_3 and HB_5 (Fig. 6b). The rupture of the initial H-bonds facilitates the exit of F^{169} from its hydrophobic pocket, allowing the loop to move towards the active

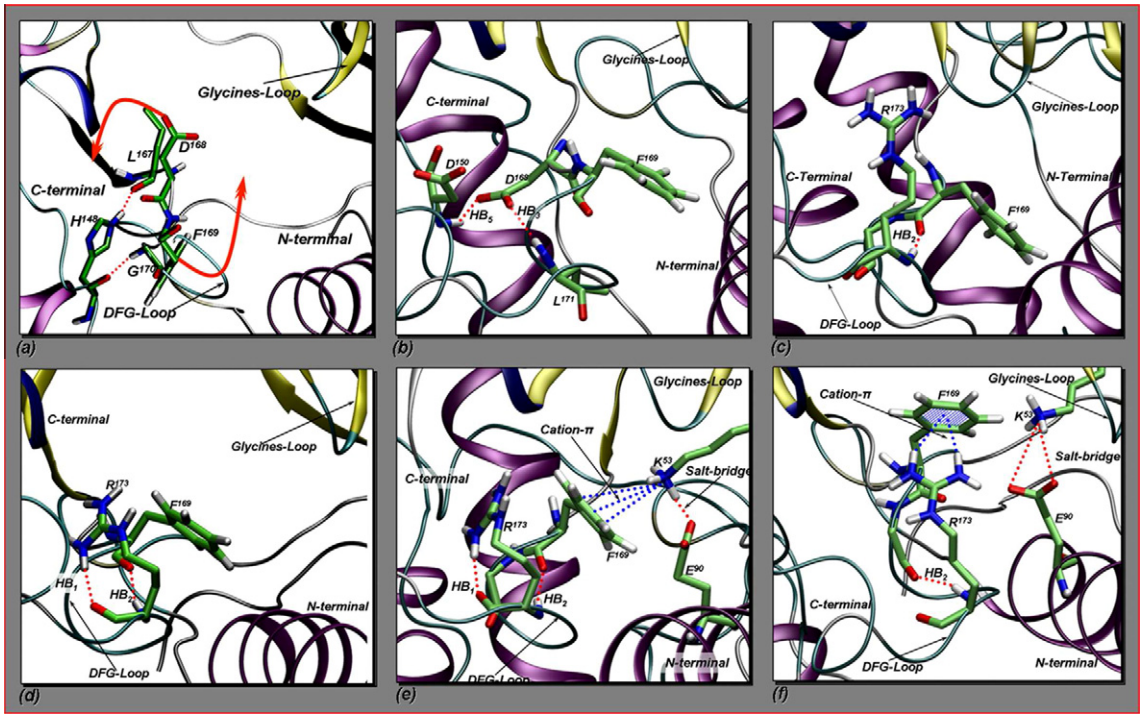

Figure 6. Mechanism proposed for the transition from the DFG-in conformation (a) to the DFG-out conformation (f) through the intermediate pseudo-DFG-out conformations (b to e). The orientation of the highlighted residues are referred to Fig. 1. The DFG-loop and the active site residues are in sticks with colour code: C atoms: green; N atoms: blue; O atoms: red; H atoms white. H-bonds are indicated with red dotted lines; cation–π interactions are indicated with blue dotted lines. The orange arrows in (a) point out the directions of the applied vectors.

site cavity interior. At this stage, the DFG-loop is in the pseudo-DFG-out conformation and F^{169} is exposed to the solvent. R^{173} is also involved in this rearrangement: the flexibility of its side-chain allows first the formation of the HB_2 interaction (Fig. 6c) and subsequently the formation of the intra-residue H-bond HB_1 (Fig. 6d). It is worth noting that HB_1 plays a relevant role in the transition, since it promotes the R^{173} side-chain bending that, in this way, shields F^{169} from the water molecules. This action is assisted by K^{53} (Fig. 6e), whose cationic head makes a cation–π interaction with the F^{169} ring, thus increasing the capability of the F^{169} ring to be solvated.[29,30] R^{173} competes with the K^{53} for establishing a cation–π interaction with F^{169}: the establishment of the R^{173} – F^{169} cation–π interaction promotes the F^{169} side chain rotation and causes the loss of both the K^{53} – F^{169} cation–π interaction and the HB_1. In the final step, the cation–π interaction between R^{173} and F^{169} is maximized, while K^{53} is involved in charge-reinforced H-bonds with the side-chain of the nearby residue E^{71} (Fig. 6f). In the literature, experimental evidences are given to support the higher frequency of Phe-Arg couples versus Lys-Phe couples.[31] This is justified by the expectation that aromatic rings, being delocalised and innately hydrophobic, will interact preferably with cations characterised by charge delocalization: thus Arg is preferred over Lys because its guanidinium group is a delocalized systems and therefore it is, at least to some extent, relatively hydrophobic.

In the depicted mechanism, a primary role seems thus to be played by the side-chain of F^{169} and its capability to form cation–π interactions with positively charged residues. In fact, the K^{53} – F^{169} cation–π interaction stabilizes the pseudo-DFG-out intermediate, where the hydrophobic F^{169} side-chain is solvent exposed, and its interplay and competition with a second cation–π couple (R173-F^{169}) promotes the subsequent transition to the DFG-out.

4.2. Implications for type-II ligand binding

A detailed analysis of trajectories docked with allosteric inhibitors shows that the aromatic moieties constituting the inhibitor backbone may act as chaperons for F^{169} rotation: each aromatic ring interacts successively via π-stacking with the F^{169} side chain assisting the flip of the loop. This is shown in Fig. 7 where snapshots of the trajectories of the complex between the p38α enzyme and the type-II inhibitor from the PDBID: 1WBT are reported. The establishment of the hydrogen bond interactions between the donor/acceptor amide moiety and the E^{71} and D^{168} enzyme residues, mandatory

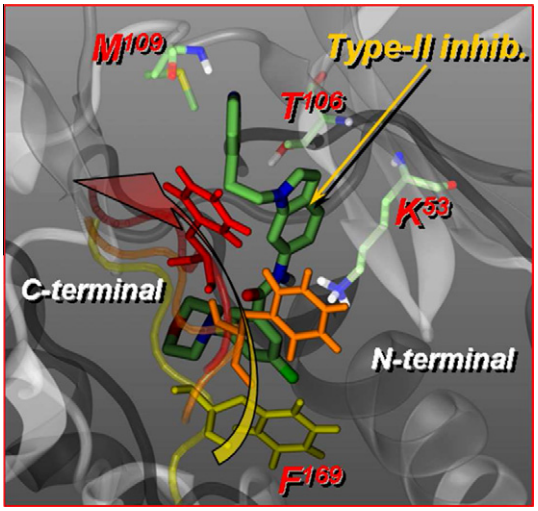

Figure 7. Type-II inhibitor BIRB796 docked into three MD trajectory snapshots illustrating the first steps of the DFG flip. The final DFG-out conformation is not shown.

for kinases inhibition, force the aryl-core of the substituent to interfere sterically with the F^{169} side-chain (F^{169} residue coloured in yellow in Fig. 7). This is removed from its buried position and pushed to the pseudo-DFG-out conformation, where the aromatic side-chain coordinates the K^{53} residue through a cation–π interaction (orange F^{169} residue in Fig. 7); afterward, F^{169} climbs the inhibitor toward the solvent (red F^{169} residue in Fig. 7), assisted by the interactions with other residues belonging to the activation loop, as described in the Transition Mechanism paragraph.

5. Conclusion

This work is based on the assumption that the conformational change of the activation loop is induced by the presence of allosteric inhibitors in the binding cavity in agreement with recently published findings which support the idea that it is more probable for allosteric inhibitors to bind first a DFG-in protein and then turn it into a DFG-out state than to encounter a free protein in the DFG-out conformation and directly bind to it.

The DFG-in to DFG-out mechanism proposed here describes at atomic detail the activation loop transition from a known (experimentally determined) initial conformation to a known (experimentally determined) final transition. The results of the AMD simulation performed support the existence of a persistent conformation, the pseudo-DFG-out, which is intermediate between the DFG-in and the DFG-out conformations, in agreement with recent computational and experimental research studies that clearly highlight the existence of intermediate conformations for the MAP-Ks, which could be the route to entry for allosteric inhibitors.

Most importantly, besides the role played by several hydrogen bond interactions, cation–π interactions involving the DFG-loop residue F^{169} seem to be involved in the DFG conformational change, promoting the transition of the whole activation loop to its final DFG-out state. Key to this mechanism is the increased hydrophilicity of F^{169} side-chain when involved in a cation–π adduct.

The detailed information obtained from this study on the network of residues involved in the framework of the mechanism proposed can be exploited to guide further site-directed mutagenesis and drug design studies.

References and notes

1. Adams, J.; Badger, A.; Kumar, S.; Lee, J. *Prog. Med. Chem.* **2001**, *38*, 1.
2. Pearson, G.; Robinson, F.; Beers Gibson, T.; Xu, B.; Karandikar, M.; Berman, K.; Cobb, M. *Endocr. Rev.* **2001**, *22*, 153.
3. Subramanian, J.; Sharma, S.; B-Rao, C. *ChemMedChem* **2008**, *3*, 336.
4. Kornev, A.; Haste, N.; Taylor, S.; Ten Eyck, L. *Proc. Natl. Acad. Sci. U.S.A.* **2006**, *103*, 17783.
5. Bernstein, F.; Koetzle, T.; Williams, G.; Meyer, E., et al *Arch. Biochem. Biophys.* **1978**, *185*, 584.
6. Wilson, K.; McCaffrey, P.; Hsiao, K.; Pazhanisamy, S.; Galullo, V.; Bemis, G.; Fitzgibbon, M.; Caron, P.; Murcko, M.; Su, M. *Chem. Biol.* **1997**, *4*, 423.
7. Gill, A.; Frederickson, M.; Cleasby, A.; Woodhead, S.; Carr, M.; Woodhead, A.; Walker, M.; Congreve, M.; Devine, L.; Tisi, D., et al *J. Med. Chem.* **2005**, *48*, 414.
8. Zuccotto, F.; Ardini, E.; Casale, E.; Angiolini, M. *J. Med. Chem.* **2010**, *53*, 2681.
9. Kufareva, I.; Abagyan, R. *J. Med. Chem.* **2008**, *51*, 7921.
10. Simard, J.; Getlik, M.; Grutter, C.; Schneider, R.; Wulfert, S.; Rauh, D. *J. Am. Chem. Soc.* **2010**, *132*, 4152.
11. Zhou, T.; Commodore, L.; Huang, W.; Wang, Y.; Sawyer, T.; Shakespeare, W.; Clackson, T.; Zhu, X.; Dalgarno, D. *Chem. Biol. Drug Des.* **2010**, *75*, 18.
12. Liu, Y.; Gray, N. *Nat. Chem. Biol.* **2007**, *2*, 358.
13. Okram, B.; Nagle, A.; Adrián, F.; Lee, C.; Ren, P.; Wang, X.; Sim, T.; Xie, Y.; Wang, X.; Xia, G.; Spraggon, G.; Warmuth, M.; Liu, Y.; Gray, N. *Chem. Biol.* **2006**, *13*, 779.
14. Angell, R.; Angell, T.; Bamborough, P.; Bamford, M.; Chung, C.; Cockerill, S.; Flack, S.; Jones, K.; Laine, D.; Longstaff, T., et al *Bioorg. Med. Chem. Lett.* **2008**, *18*, 4433.
15. Vogtherr, M.; Saxena, K.; Hoelder, S.; Grimme, S.; Betz, M.; Schieborr, U.; Pescatore, B.; Robin, M.; Delarbre, L.; Langer, T.; Wendt, K. U.; Schwalbe, H. *Angew. Chem., Int. Ed.* **2006**, *45*, 993.
16. Frembgen-Kesner, T.; Elcock, A. *J. Mol. Biol.* **2006**, *359*, 202.
17. Shana, Y.; Seeliger, M. A.; Eastwood, F.; Frank, M. P.; Xua, H.; Jensena, M. O.; Drora, R. O.; Kuriyan, J.; Shaw, D. *Proc. Natl. Acad. Sci. U.S.A.* **2009**, *106*, 139.
18. Bukhtiyarova, M.; Karpusas, M.; Northrop, K.; Namboodiri, H. V. M.; Springman, E. B. *Biochemistry* **2007**, *46*, 5687.
19. Sullivan, J.; Holdgate, G.; Campbell, D.; Timms, D.; Gerhardt, S.; Breed, J.; Breeze, A.; Bermingham, A.; Pauptit, R.; Norman, R., et al *Biochemistry* **2005**, *44*, 16475.
20. Simard, J.; Getlik, M.; Grutter, C.; Pawar, V.; Wulfert, S.; Rabiller, M.; Rauh, D. *J. Am. Chem. Soc.* **2009**, *131*, 13286.
21. Simard, J.; Grutter, C.; Pawar, V.; Aust, B.; Wolf, A.; Rabiller, M.; Wulfert, S.; Robubi, A.; Kluter, S.; Ottmann, C., et al *J. Am. Chem. Soc.* **2009**, *131*, 18478.
22. Lindahl, E.; Hess, B.; van der Spoel, D. *J. Mol. Model.* **2001**, *7*, 306.
23. Berendsen, H.; Van der Spoel, D.; Van Drunen, R. *Comp. Phys. Commun.* **1995**, *91*, 43.
24. van der Spoel, D.; Lindahl, E.; Hess, B.; van Buuren, A. R.; Apol, E.; Meu-lenhoff, P. J.; Tieleman, D. P.; Sijbers, A. L. T. M.; Feenstra, K. A.; van Drunen, R.; Berendsen, H. J. C. Gromacs User Manual Version. http://www.gromacs.org, 2005.
25. Url = http://accelrys.com/products/quanta/index.html, 2006.
26. Hess, B.; Bekker, H.; Berendsen, H.; Fraaije, J. *J. Comp. Chem.* **1997**, *18*, 1463.
27. Brooks, B. R.; Bruccoleri, R. E.; Olafson, B. D.; States, D. J.; Swaminathan, S.; Karplus, M. *J. Comp. Chem.* **1983**, *4*, 187.
28. Url = http://accelrys.com/products/discovery-studio, 2007.
29. Costanzo, F.; Della Valle, R.; Barone, V. *J. Phys. Chem. B* **2005**, *109*, 23016.
30. Rao, J. S.; Zipse, H.; Sastry, G. N. *J. Phys. Chem. B* **2009**, *113*, 7225.
31. Dougherty, D. *J. Nutr.* **2007**, *137*, 1504S.
32. Humphrey, W.; Dalke, A.; Schulten, K. *J. Mol. Graphics* **1996**, *14*, 33.